Conformational Differences between *Azotobacter vinelandii* Nitrogenase MoFe Proteins As Studied by Small-Angle X-ray Scattering†

Mary C. Corbett,‡ Yilin Hu,§ Aaron W. Fay,§ Hiro Tsuruta,|| Markus W. Ribbe,*,§ Keith O. Hodgson,*,‡,|| and Britt Hedman*,||

Department of Chemistry, Stanford University, Stanford, California 94305-5080, Department of Molecular Biology and Biochemistry, University of California, Irvine, California 92697-3900, and Stanford Synchrotron Radiation Laboratory, SLAC, Stanford University, 2575 Sand Hill Road, MS 69, Menlo Park, California 94025-7015

Received March 13, 2007; Revised Manuscript Received April 17, 2007

ABSTRACT: The nitrogenase MoFe protein is a heterotetramer containing two unique high-nuclearity metalloclusters, FeMoco and the P-cluster. FeMoco is assembled outside the MoFe protein, whereas the P-cluster is assembled directly on the MoFe protein polypeptides. MoFe proteins isolated from different genetic backgrounds have been analyzed using biochemical and spectroscopic techniques in attempting to elucidate the pathway of P-cluster biosynthesis. The Δ*nifH* MoFe protein is less stable than other MoFe proteins and has been shown by extended X-ray absorption fine structure studies to contain a variant P-cluster that most likely exists as two separate $[Fe_4S_4]$-like clusters instead of the subunit-bridging $[Fe_8S_7]$ cluster found in the wild-type and Δ*nifB* forms of the MoFe protein [Corbett, M. C., et al. (2004) *J. Biol. Chem. 279*, 28276−28282]. Here, a combination of small-angle X-ray scattering and Fe chelation studies is used to show that there is a correlation between the state of the P-cluster and the conformation of the MoFe protein. The Δ*nifH* MoFe protein is found to be larger than the wild-type or Δ*nifB* MoFe proteins, an increase in size that can be modeled well by an opening of the subunit interface consistent with P-cluster fragmentation and solvent exposure. Importantly, this opening would allow for the insertion of P-cluster precursors into a region of the MoFe protein that is buried in the wild-type conformation. Thus, Δ*nifH* MoFe protein could represent an early intermediate in MoFe protein biosynthesis where the P-cluster precursors have been inserted, but P-cluster condensation and tetramer stabilization have yet to occur.

The nitrogenase enzyme system represents an excellent target for studying the assembly of complex metalloproteins because its maturation process includes a variety of biosynthetic strategies, including "in situ" and "ex situ" cluster assembly (*1*), scaffold proteins, metal cluster chaperones, and protein folding chaperonins (see reviews in refs *2*−*6*). Nitrogenase catalyzes the reduction of atmospheric dinitrogen to ammonia under ambient conditions through the combined activity of two component proteins, the MoFe protein and the Fe protein (see reviews in refs *7*−*12*).[1] In *Azotobacter vinelandii*, the catalytic nitrogenase component, the MoFe protein, is an ∼220 kDa heterotetramer consisting of homologous α- and β-subunits. The site of substrate reduction within the MoFe protein is FeMoco, a $[MoFe_7S_9X]$: homocitrate cluster,[2] which is located entirely within the α-subunit. A second metallocluster, the $[Fe_8S_7]$ P-cluster, is located at the interface of each α−β pair of the MoFe protein where it is ligated by three Cys residues from each subunit. The P-cluster presumably functions in transferring electrons from the Fe protein, the specific reductase of the MoFe protein, to FeMoco during catalysis.

FeMoco assembly occurs independent of the MoFe protein in a stepwise process requiring several *nif* gene products. Significant progress has been made in elucidating the nature of FeMoco at different stages in this process (*1*, *13*, *14*). Less well characterized is the assembly of the P-cluster, a

† This work was supported by NIH Grants RR-01209 (K.O.H.) and GM-67626 (M.W.R.). Scattering data were measured at SSRL, which is supported by the DOE, Office of Basic Energy Sciences. The SSRL Structural Molecular Biology Program is supported by the NIH, National Center for Research Resources, Biomedical Technology Program, and by the DOE, Office of Biological and Environmental Research.

* To whom correspondence should be addressed. M.W.R.: e-mail, mribbe@uci.edu; phone, (949) 824-9509; fax, (949) 824-8551. K.O.H.: e-mail, hodgson@ssrl.slac.stanford.edu; phone, (650) 926-3153; fax, (650) 926-4100. B.H.: e-mail, hedman@ssrl.slac.stanford.edu; phone, (650) 926-3052; fax, (650) 926-4100.

‡ Department of Chemistry, Stanford University.

§ University of California.

|| Stanford Synchrotron Radiation Laboratory, SLAC, Stanford University.

[1] There are at least three highly related families of nitrogenase proteins distinguished by the metal contents of their active sites (*33*, *46*). The Mo-containing system discussed herein is considered to be the "conventional" nitrogenase. A fourth, unrelated, superoxide-dependent system also exists (*47*).

[2] X represents a light atom of unknown identity, which may be C, O, or N (*48*).

[3] Abbreviations: EXAFS, extended X-ray absorption fine structure; Δ*nifB* MoFe protein, FeMoco-deficient, wild-type P-cluster-containing MoFe protein, which is expressed in the absence of the *nifB* gene, a gene specific to FeMoco biosynthesis; Δ*nifH* MoFe protein, FeMoco-deficient, P-cluster variant-containing MoFe protein, which is expressed in the absence of the *nifH* gene, the gene encoding the Fe protein; $\Delta nifH^{pi}$ MoFe protein, form of Δ*nifH* MoFe protein that has been pre-incubated with Fe protein and MgATP prior to purification; SAXS, small-angle X-ray scattering; SSRL, Stanford Synchrotron Radiation Laboratory; R_g, radius of gyration; $p(r)$, electron pair distance distribution function; D_{max}, maximum particle dimension.

10.1021/bi7005064 CCC: $37.00
Published on Web 06/14/2007

process that takes place, at least partially, on the MoFe protein polypeptides. It was recently shown that the P-cluster can be structurally characterized through extended X-ray absorption fine structure (EXAFS)[3] analysis of FeMoco-deficient MoFe proteins produced by the deletion of genes required for FeMoco biosynthesis (*15*). When the *nifB* gene is deleted, the resulting MoFe protein (designated Δ*nifB* MoFe protein) is FeMoco-deficient, but capable of being reconstituted with isolated FeMoco, and contains spectroscopically and structurally defined wild-type P-clusters (*15*−*18*). In contrast, when the *nifH* gene is deleted, the resulting MoFe protein (designated Δ*nifH* MoFe protein) is FeMoco-deficient, incapable of reconstitution and, although it contains sufficient Fe to form the P-clusters, exhibits a distinct $S = {}^1/_2$ EPR signal and an EXAFS pattern consistent with the presence of $[Fe_4S_4]$-like P-cluster variants (*15*, *18*, *19*). Studies of Δ*nifH* MoFe protein in different states, and in comparison with other nitrogenase proteins exhibiting the same $S = {}^1/_2$ EPR signal, strongly suggest that the P-cluster variant in Δ*nifH* MoFe protein is not a subunit-bridging eight-Fe cluster but is instead fragmented with a single four-Fe cluster on each subunit (*15*, *19*).

Because P-cluster variants are observed when the *nifH* gene is deleted, experiments were conducted to ascertain whether Fe protein, the *nifH* gene product, was capable of transforming the P-cluster variants on Δ*nifH* MoFe protein into wild-type P-clusters. In these experiments, Fe protein and MgATP were preincubated with the crude extract of an *A. vinelandii* Δ*nifH* strain prior to purification of the MoFe protein (designated Δ*nifH*^{PI} MoFe protein) (*19*). EPR and EXAFS analyses of Δ*nifH*^{PI} MoFe protein indicate that a wild-type P-cluster was not formed during the preincubation reaction; however, unlike Δ*nifH* MoFe protein, Δ*nifH*^{PI} MoFe protein is capable of partial reconstitution with isolated FeMoco (*19*). These results imply that the Fe protein (NifH) may be involved in two distinct functions during MoFe protein maturation: (i) opening the α-subunit for FeMoco insertion and (ii) assisting in P-cluster formation across the α subunit−β subunit interface. The inability of Fe protein to function in the latter role during the preincubation experiment suggests that P-cluster formation may occur early in the biosynthetic process, potentially during MoFe protein tetramer assembly. If so, MoFe proteins having P-cluster variants might be expected to have conformations different from those with a wild-type P-cluster.

Small-angle X-ray scattering (SAXS) studies, which provide shape information about proteins in solution, are described herein that probe whether there is a correlation between P-cluster state and MoFe protein conformation. The SAXS profiles of four different MoFe proteins are analyzed: wild-type MoFe protein, Δ*nifB* MoFe protein, Δ*nifH* MoFe protein, and Δ*nifH*^{PI} MoFe protein. Because Δ*nifH* MoFe protein is FeMoco-deficient in addition to having variant P-clusters, a direct comparison cannot be made with the wild-type MoFe protein. Comparison of the wild-type and Δ*nifB* MoFe proteins is included to demonstrate the impact of FeMoco on the MoFe protein SAXS data, as this has not been addressed (*20*, *21*). We studied the Δ*nifH*^{PI} MoFe protein to determine whether MoFe protein conformational change occurs in this protein independent of P-cluster assembly. This is shown not to be the case as the scattering profiles from the Δ*nifH* and *nifH*^{PI} MoFe proteins are found to be extremely similar.

Further structural evidence of MoFe protein conformation is provided by an Fe chelation assay, which probes the solvent accessibility of the Fe atoms in the P-cluster. Together, the SAXS and chelation studies show that the P-cluster variant-containing Δ*nifH* MoFe protein is larger than both the wild-type and Δ*nifB* MoFe proteins, consistent with an opening of the α subunit−β subunit interface.

MATERIALS AND METHODS

Cell Growth and Protein Purification. All *A. vinelandii* strains were grown in 180 L batches in a 200 L New Brunswick fermentor on Burke's minimal medium supplemented with 2 mM ammonium acetate. The growth rate was measured by cell density at 436 nm using a Spectronic 20 Genesys Spectrophotometer. After ammonia consumption, the cells were de-repressed for 3 h followed by harvesting using a flow-through centrifugal harvester. The cell paste was washed with 50 mM Tris-HCl (pH 8.0). Published methods were used for the purification of wild-type *A. vinelandii* MoFe protein (MoFe protein) (*22*) and the His-tagged MoFe proteins expressed by *A. vinelandii* DJ1143 (Δ*nifB* MoFe protein) (*18*) and DJ1165 (Δ*nifH* MoFe protein) (*18*). Δ*nifH*^{PI} MoFe protein, which is expressed by an *A. vinelandii* DJ1165 strain preincubated with the Fe protein and MgATP, was prepared as described previously (*19*). All protein samples were prepared in a Vacuum Atmospheres Ar-filled drybox with <4 ppm O_2 and concentrated in a Centricon-30 (Amicon) concentrator in anaerobic centrifuge tubes outside the drybox to final stock concentrations of 15.5 mg/mL MoFe protein, 11.9 mg/mL Δ*nifB* MoFe protein, 13.3 mg/mL Δ*nifH* MoFe protein, and 21.6 mg/mL Δ*nifH*^{PI} MoFe protein.

Sample Preparation. Samples for SAXS analysis in 25 mM Tris-HCl (pH 8.0), 250 mM imidazole, 500 mM NaCl, 2 mM $Na_2S_2O_4$, and 10% glycerol were frozen and then shipped to the Stanford Synchrotron Radiation Laboratory (SSRL) on dry ice. Samples were thawed in the antichamber of a N_2-filled Vacuum Atmospheres drybox and then maintained at <5 ppm O_2 inside the drybox. The samples were either shipped prediluted or diluted in the drybox with O_2-free buffer. In some cases, NaCl was added to increase the NaCl concentration of the solutions to 750 mM. The samples were loaded into 1.2 mm, 15 μL polycarbonate cells with 0.025 mm Mica (Goodfellow) windows. The solution cell loading ports were sealed with modeling clay and then transported to the beamline under N_2. To maintain an O_2-limited atmosphere during data collection, a stream of N_2 gas was positioned over the sample cell ports. The protein samples did not show any signs of O_2 damage when the equipment was functioning properly. When the scattering profile changed rapidly during data collection, O_2 damage was suspected and the experiments were repeated with fresh samples. Following data collection, concentrations were determined by absorbance at 280 nm.

A buffer solution consisting of 25 mM Tris-HCl (pH 8.0), 250 mM imidazole, 2 mM $Na_2S_2O_4$, 10% glycerol, and either 500 or 750 mM NaCl was measured before and after each protein solution in the same polycarbonate cell used to measure the protein. A 5.1 mg/mL solution of bovine serum

albumin (Fisher, fraction V, cold alcohol precipitated) in 25 mM Tris-HCl (pH 8.0), 250 mM imidazole, 500 mM NaCl, 2 mM $Na_2S_2O_4$, and 10% glycerol was measured as a molecular mass standard (molecular mass = 69 kDa; R_g = 31.3 Å).

SAXS Data Collection. SAXS data were collected at SSRL under 3 GeV, 70−100 mA beam conditions using the 20-pole, 0.66 T wiggler beam line 4-2 with a Si(111) monochromator and a Pt-coated bent cylindrical mirror for beam focusing and harmonic rejection above 11 keV (*23, 24*). The beam size at the sample was defined to be 0.2 mm × 1.0 mm, or smaller, in full width at half-maximum. The X-ray energy was calibrated to 8.98 keV using a standard Cu foil. Samples were maintained at 15 °C during data collection by using a chilled holder. A MarCCD 165 detector was used to record the scattered radiation. The detector channel numbers were converted to momentum transfer h, where $h = 4\pi \sin(\theta)/\lambda$, 2θ is the scattering angle, and λ is the wavelength (1.38 Å), by using the (100) reflection from a cholesterol myristate powder sample as a standard. Scattering data were collected over 5−20 min in 10 s intervals. Individually intensity-scaled and azimuthally averaged one-dimensional scattering curves were compared on the basis of the variance among 10−20 buffer data frames collected just prior to or just after the data frames. This variance is representative for the overall systematic error; therefore, only those protein scattering curves that were within the buffer variance multiplied by a factor of 1.5 were averaged together. The effects of X-ray or O_2 damage were limited by including in the average only those data frames that did not significantly differ from the first 10 s frame in a series. To obtain radius of gyration (R_g) information, which provides a good estimate of particle size, and to check for concentration-dependent effects, dilute samples (1−4 mg/mL) were measured at a long detector distance, 2.5 m. To obtain the more detailed shape information available at higher values of h, concentrated samples (11−16 mg/mL) were measured at a shorter detector distance, 1.0 m.

SAXS Data Analysis. The raw scattering data were processed by using MarParse, a SSRL-developed software program for scaling and circularly integrating the two-dimensional CCD detector data to one-dimensional data (*24*), and *PRIMUS* (*25*) for buffer subtraction. To compare data from different runs, the calibrant scattering profiles were overlaid to determine the factors for scaling scattered intensity. Scattering data were also scaled by concentration as noted in the text.

There were not sufficient points in the overlap region between the low- and intermediate-range data sets to allow for the construction of merged data sets; therefore, the two types of data were analyzed separately. For dilute protein solutions (1−4 mg/mL), *PRIMUS* (*25*) was used to determine R_g values using the Guinier approximation over a consistent range, where $h_{min} \leq \pi/D_{max}$ (D_{max} is the maximum particle dimension) and $h_{max}R_g \leq 1.3$. To test the impact of the range of h on R_g determination, a representative wild-type MoFe protein data set was fit over several different ranges. The resulting R_g values were spread over 1.7 Å, but there was no apparent trend of increasing or decreasing R_g with an increasing h range. For all of the proteins that were measured, R_g values were reproducible to within 2% when the protein concentration was ≤4 mg/mL, even when data from different runs, with different NaCl concentrations, and with different protein concentrations were considered.

The program *GNOM* (*26*) was used to calculate $p(r)$ functions from SAXS data over an h range of 0.02−0.1 Å^{-1} by an indirect transform method. The $p(r)$ function was constrained to be 0 at D_{max}. D_{max} values were determined by iteratively searching for the lowest value that provided a good visual match to the scattering data in reciprocal space, reasonable real space features, and an optimal value for the regularization parameter. Using *GNOM*, R_g values were calculated from $p(r)$ functions (*26*). As a wider data range is used for the evaluation of R_g by this method, the values are considered to be less sensitive to interparticle interference effects or trace aggregates and, therefore, more reliable (*27*).

To analyze the solution scattering data in the intermediate-h range, data over the interval of 0.04−0.30 Å^{-1} were compared to scattering profiles calculated from crystallographic coordinates using *CRYSOL* (*28*). Given atomic coordinates, *CRYSOL* computes the theoretical scattering intensities, $I_c(h)$, including a hydration shell, and then fits the experimental intensities, $I_e(h)$, by adjusting the excluded volume and the contrast of the hydration shell to minimize the function χ^2 (defined in eq 1)

$$\chi^2 = \frac{1}{N}\sum_{i=1}^{N}\left[\frac{I_e(h_i) - cI_c(h_i)}{\sigma(h_i)}\right]^2 \quad (1)$$

where N is the number of experimental points, $\sigma(h_i)$ values are the experimental errors, and c is a scale factor that includes the varied parameters (*28*).

Atomic coordinates were obtained from the deposited structures of wild-type MoFe protein [PDB entry 3MIN (*29*)] and Δ*nifB* MoFe protein [PDB entry 1L5H (*17*)]. *PyMOL* (*30*) was used to create a suite of MoFe protein structures to represent the Δ*nifH* MoFe protein structure in which the subunits of a FeMoco-deleted form of the wild-type structure were translated and/or rotated with respect to each other. Subunit translations were iteratively checked against the Δ*nifH* MoFe protein scattering data using *CRYSOL* (*28*) in 1 Å increments and domain rotations in 5° increments, where domains were defined as described in ref *31*. Combinations of translations and rotations were also tested.

Fe Chelation Assay. The Fe chelation assay provides a biochemical probe of the solvent accessibility of the P-cluster Fe atoms in the FeMoco-deficient MoFe proteins.[4] In this assay, a 1.3 mg/mL protein solution was prepared in an anaerobic cuvette inside an Ar-filled Vacuum Atmospheres drybox at <2 ppm O_2. The visible region absorption of this solution was measured as a blank spectrum using a Thermo Spectronic (Shelton, CT) Genesys 6 spectrophotometer, after which the chelator, bathophenanthroline disulfonate (2 mM), was added to the cuvette to initiate the reaction (*32*). The total amount of chelation was measured by monitoring the absorption of the Fe−bathophenanthroline complex at 535 nm.

[4] Only FeMoco-deficient MoFe proteins were examined with the Fe chelation assay because wild-type MoFe protein contains a different amount of Fe than Δ*nifH* MoFe protein.

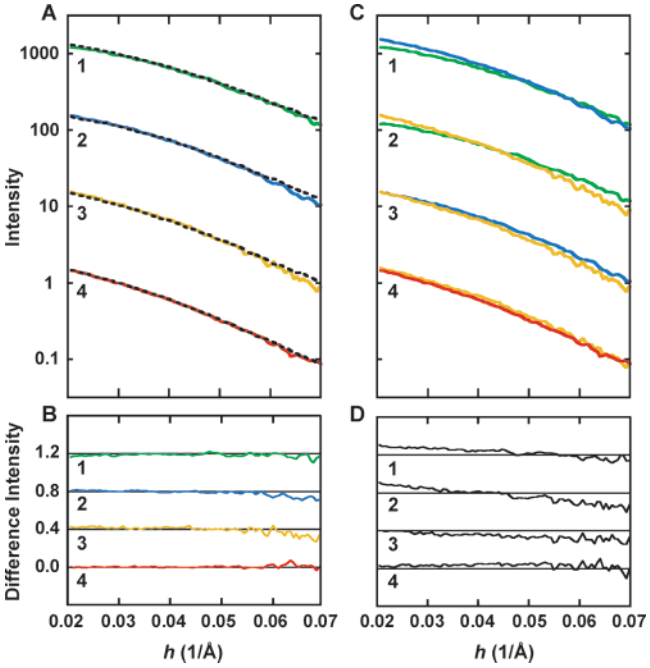

FIGURE 1: SAXS comparisons of wild-type (green), Δ*nifB* (blue), Δ*nifH* (gold), and Δ*nifH*^{PI} (red) MoFe proteins at low *h* values (2.5 m detector distance). (A) Offset scattering profiles of MoFe proteins at two different concentrations scaled to represent concentrations of 1 mg/mL: (1) 1.9 mg/mL wild-type MoFe protein (green) and 3.7 mg/mL wild-type MoFe protein (black), (2) 2.0 mg/mL Δ*nifB* MoFe protein (blue) and 3.9 mg/mL Δ*nifB* MoFe protein (black), (3) 1.5 mg/mL Δ*nifH* MoFe protein (gold) and 3.3 mg/mL Δ*nifH* MoFe protein (black), and (4) 1.9 mg/mL Δ*nifH*^{PI} MoFe protein (red) and 4.0 mg/mL Δ*nifH*^{PI} MoFe protein (black). (B) Offset difference intensity profiles for the scattering profiles in panel A. Note that concentration-dependent effects are not significant between *h* values of 0.02 and 0.06 Å^{-1}. (C) Offset scattering profiles of the ~2 mg/mL MoFe protein solutions in panel A, colored as in panel A. (D) Offset difference intensity profiles for the scattering profiles in panel C.

RESULTS

Small-Angle Region. To minimize the impact of negative effects on the data in the lowest angular region, such as poor signal-to-noise levels, mild interparticle interference effects, and incomplete background subtractions, the SAXS data were consistently analyzed over a single angular range that afforded the best comparison between the different proteins. As shown in panels A and B of Figure 1, the differences between two concentrations of the same protein are minimal in the low-angle region that was analyzed. In accordance with these results, R_g values calculated either using the Guinier approximation [*PRIMUS* (*25*)] or from *p*(*r*) functions [*GNOM* (*26*)] are the same within error (Table 1). An excellent level of internal consistency in the data is also demonstrated by the *I*(0) values, which scale linearly with concentration, and the protein molecular weights, calculated using a bovine serum albumin standard, which are within ~15% of the expected value.

The comparisons between two concentrations of the same protein provide a baseline for assessing the subtle differences between the various MoFe proteins. The wild-type MoFe protein scattering profile clearly differs from those of both types of FeMoco-deficient proteins, Δ*nifB* and Δ*nifH* MoFe proteins (Figure 1C,D). The flatter slope of the wild-type MoFe protein data corresponds to its lower value for R_g relative to the other MoFe proteins. The R_g value determined for the wild-type MoFe protein of 40.2 Å (Table 1) matches well with the theoretical value of ~39 Å calculated from the MoFe protein crystal structure (*29*). Δ*nifB* MoFe protein is slightly bigger than the wild-type MoFe protein, having an R_g value of 42.4 Å (Table 1). The small, but reproducible, difference in R_g values between these two types of MoFe proteins is likely due to the differences in the conformations of their α-subunits: Δ*nifB* MoFe protein is poised in an "open" conformation in which one of the domains in the α-subunit is substantially shifted to accommodate insertion of FeMoco (*17*).

Table 1: Shape Parameters of Nitrogenase Proteins[a]

	average R_g (Å) (*PRIMUS*)[b]	R_g (Å) (*GNOM*)[c]	D_{max} (Å)
wild-type MoFe	40.2	40.2	117
Δ*nifB* MoFe	42.5	42.4	121
Δ*nifH* MoFe	46.2	45.7	132
Δ*nifH*^{PI} MoFe	47.0	46.0	130

[a] Errors are estimated to be 1−2% for R_g values and 5% for D_{max} values. [b] R_g values determined by the Guinier approximation using *PRIMUS* (*25*) are averages from six or seven independently measured and analyzed protein solutions of each type with concentrations between 1 and 4 mg/mL. [c] R_g values determined using *GNOM* (*26*) from *p*(*r*) functions calculated from fits to the scattering data of the ~2 mg/mL protein solutions shown in Figure 1.

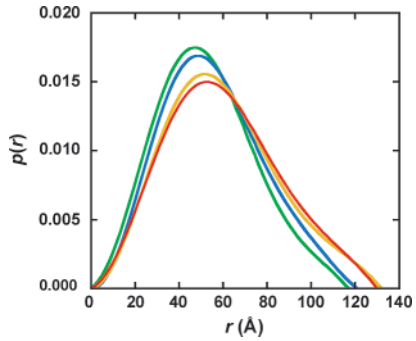

FIGURE 2: Distance distribution functions [*p*(*r*)] of wild-type (green), Δ*nifB* (blue), Δ*nifH* (gold), and Δ*nifH*^{PI} (red) MoFe proteins. *p*(*r*) values were calculated using *GNOM* (*26*) from fits to the ~2 mg/mL scattering data shown in Figure 1. The curves are normalized to have a total area of 1.

The R_g value of the Δ*nifH* MoFe protein at ~46 Å is larger than that of both the wild-type and Δ*nifB* MoFe proteins (Table 1), and whereas the wild-type and Δ*nifB* MoFe proteins have a *p*(*r*) peak at ~48 Å, the Δ*nifH* MoFe protein *p*(*r*) peaks at ~52 Å (Figure 2). In the case of a globular protein such as the MoFe protein, the *p*(*r*) peak position depends very little on the choice of D_{max}, which can be sensitive to the presence of trace aggregates or flexible residues around the periphery of the molecule. These differences thus unequivocally signify that Δ*nifH* MoFe protein is in an extended conformation compared to the wild-type protein. Cys alkylation experiments have shown that Cysα275, the Cys residue that provides a ligand to FeMoco in the wild-type MoFe protein, is exposed to solvent in the Δ*nifB* MoFe protein, but not in the wild-type or Δ*nifH* MoFe proteins (*33*). This result presumably indicates that the rearrangement of the α-subunit observed in the Δ*nifB* MoFe protein has not taken place in the Δ*nifH* MoFe protein, consistent with the inability to reconstitute purified Δ*nifH* MoFe protein with isolated FeMoco (*18*). Therefore, the

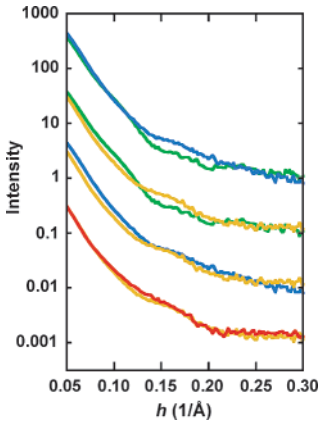

FIGURE 3: SAXS comparisons of wild-type (green), Δ*nifB* (blue), Δ*nifH* (gold), and Δ*nifH*^{PI} (red) MoFe proteins at intermediate *h* values (1 m detector distance). The scattering profiles are scaled to represent a concentration of 1 mg/mL and are offset for clarity.

observed differences in R_g (Table 1) and in the $p(r)$ functions (Figure 2) between the wild-type and Δ*nifH* MoFe proteins must be due to a rearrangement different from that observed in the Δ*nifB* MoFe protein and are likely related to the lack of a subunit-bridging P-cluster in Δ*nifH* MoFe protein (*15*).

The scattering profile of Δ*nifH*^{PI} MoFe protein is remarkably similar to that of Δ*nifH* MoFe protein (Figure 1C,D). Consequently, Δ*nifH*^{PI} MoFe protein is found to have an R_g value (Table 1) and $p(r)$ features (Figure 2) similar to those of Δ*nifH* MoFe protein. Δ*nifH*^{PI} MoFe protein is only partially activated after reconstitution with FeMoco, which indicates that it may exist as a mixture of conformers, including some with an open α-subunit (*19*). The shape parameters reported herein indicate that the dominant conformation of the Δ*nifH*^{PI} MoFe protein is largely unchanged from that of unreacted Δ*nifH* MoFe protein.

Intermediate-Angle Region. Comparison of the scattering from the various MoFe proteins between 0.05 and 0.30 Å^{-1} further highlights the differences that were apparent from the examination of the small-angle region (Figure 3). Furthermore, the data in this region reflect subtle conformational differences much more than at small angles, and as a result, they are more suitable for comparison with theoretical scattering profiles calculated from crystallographic coordinates, which can provide a correlation between differences in the scattering profiles with differences in protein structure. Unlike the small-angle region, aggregation would not be expected to impact the intermediate-*h* region of the scattering profile, even at high protein concentrations.

The wild-type MoFe protein scattering profile is matched well across the entire range analyzed by the theoretical scattering profile calculated from the unmodified wild-type MoFe protein crystal structure (Figure 4A, set 1). Comparison of the wild-type MoFe protein data with theoretical scattering profiles calculated from MoFe protein structures in which the FeMoco atoms are replaced with N atoms (Figure 4A, set 2) or removed completely (Figure 4A, set 3) indicates that the scattering in the region between 0.1 and 0.2 Å^{-1} is sensitive to the presence or absence of a heterometallic FeMoco cluster. Notably, the two FeMoco-deficient MoFe proteins differ the most from the wild-type MoFe protein in this region (Figure 3). While it was anticipated that FeMoco would have an impact on the MoFe protein scattering profile, it is surprising that the effect is so pronounced. The absence of FeMoco is not the only difference between the wild-type and Δ*nifB* MoFe proteins, however, as the theoretical scattering profile of the Δ*nifB* MoFe protein (Figure 4A, set 4) provides a worse match to the MoFe protein scattering data than that of the FeMoco-deleted form of the MoFe protein (Figure 4A, set 3). Interestingly, a form of *Klebsiella pneumoniae* MoFe protein that is naturally expressed with only half of its FeMoco sites occupied exhibits a change in scattering profile relative to that of the wild type that is similar to the differences observed here between the wild-type and Δ*nifB* forms of *A. vinelandii* MoFe protein (*21*).

Although crystallographic studies indicate that the β subunits and overall topologies of the wild-type and Δ*nifB* MoFe proteins are nearly identical, the Δ*nifB* MoFe protein has been shown to have an opening in its α subunit for accommodation of FeMoco insertion, which is formed by the rotation of one of three β-sheet−α-helical domains (see Figure 5) (*17*). The rotated domain is also more disordered, which is reflected by the missing loop between residues α381 and α408 in the crystal structure of the Δ*nifB* MoFe protein (*17*). Despite the missing residues, the theoretical scattering profile of Δ*nifB* MoFe protein provides a good match to the Δ*nifB* MoFe protein data (Figure 4B, set 1), whereas the theoretical scattering profile of wild-type MoFe protein with FeMoco deleted does not (Figure 4B, set 2).

Scattering profiles calculated from Δ*nifB* MoFe protein structures in which the P-cluster atoms were replaced with N atoms or removed (Figure 4B, sets 3 and 4) provide only moderately worse matches to the experimental data than that with the P-cluster (Figure 4B, set 1). The χ^2 values for these comparisons are increased, but the shapes of the scattering profiles are not significantly altered, indicating that the impact of the P-cluster on the Δ*nifB* MoFe protein SAXS data is minimal. FeMoco with its homocitrate ring takes up a significant volume in the α subunit; thus, its removal leaves a substantial void that affects the scattering profile of the MoFe protein. Because the P-cluster is smaller and more closely surrounded by protein residues than FeMoco, its removal has a weaker impact on the scattering properties of the MoFe protein as a whole. The lack of sensitivity to the P-cluster in the scattering profile indicates that the differences between the Δ*nifB* and Δ*nifH* MoFe protein are not simply due to changes in the P-cluster but are instead due to changes in the overall protein structure.

The Δ*nifH* MoFe protein scattering data are not matched well by theoretical scattering profiles calculated from either the Δ*nifB* or wild-type MoFe protein atomic coordinates (Figure 4C, sets 1 and 2). Comparison of the data from this FeMoco-deficient protein with that from the Δ*nifB* MoFe protein indicates that the Δ*nifH* MoFe protein has a steeper slope and that the rise in the data at 0.1−0.2 Å^{-1} is shifted to higher *h* values (Figure 3). These observations are consistent with an increase in the size of the Δ*nifH* MoFe protein relative to the Δ*nifB* MoFe protein. Because EXAFS studies suggest that the P-cluster variant of the Δ*nifH* MoFe potentially consists of isolated [Fe_4S_4]-like fragments instead of a subunit-bridging cluster (*15*), models of the Δ*nifH* MoFe protein were constructed from FeMoco-deleted wild-type MoFe protein structures in which the α and β subunits were translated with respect to each other forcing P-cluster

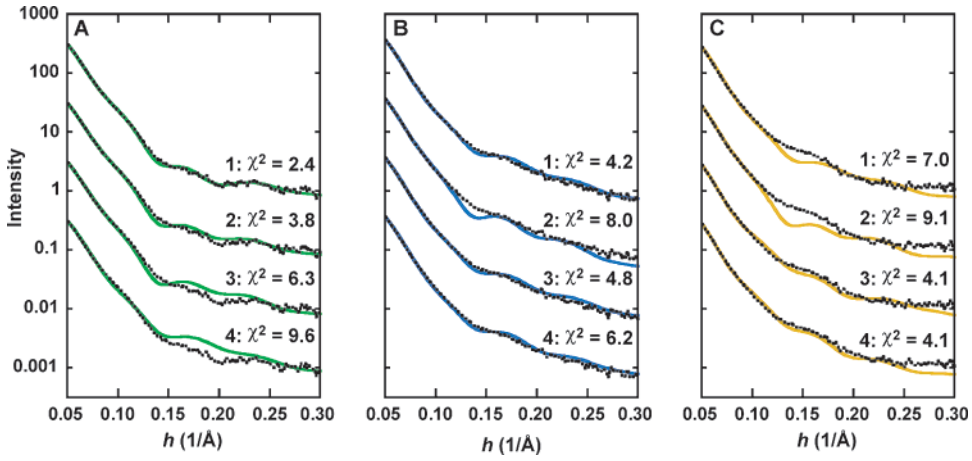

FIGURE 4: Comparison of experimental and calculated SAXS profiles of wild-type (A), Δ*nifB* (B), and Δ*nifH* (C) MoFe proteins. All proteins were scaled to a concentration of 1 mg/mL. Successive comparisons are offset for clarity. (A) Wild-type MoFe protein solution data (black) with theoretical scattering profiles (green) calculated from the atomic coordinates of wild-type MoFe protein (set 1), wild-type MoFe protein with the atoms in the FeMoco clusters replaced with N atoms (set 2), wild-type MoFe protein without FeMoco (set 3), and FeMoco-deficient Δ*nifB* MoFe protein (set 4). (B) Δ*nifB* MoFe protein solution data (black) with theoretical scattering profiles (blue) calculated from the atomic coordinates of Δ*nifB* MoFe protein (set 1), wild-type MoFe protein without FeMoco (set 2), Δ*nifB* MoFe protein with the atoms in the P-clusters replaced with N atoms (set 3), and Δ*nifB* MoFe protein without P-clusters (set 4). (C) Δ*nifH* MoFe protein solution (black) with theoretical scattering profiles (gold) calculated from the atomic coordinates of FeMoco-deficient Δ*nifB* MoFe protein (set 1), wild-type MoFe protein without FeMoco (set 2), wild-type MoFe protein without FeMoco and with a 6 Å symmetric opening of the α subunit−β subunit interface along the molecular *y*-axis (Figure 5, model 1) (set 3), and wild-type MoFe protein without FeMoco and with a 10 Å opening of the α subunit−β subunit interface along the molecular *z*-axis (Figure 5, model 2) (set 4).

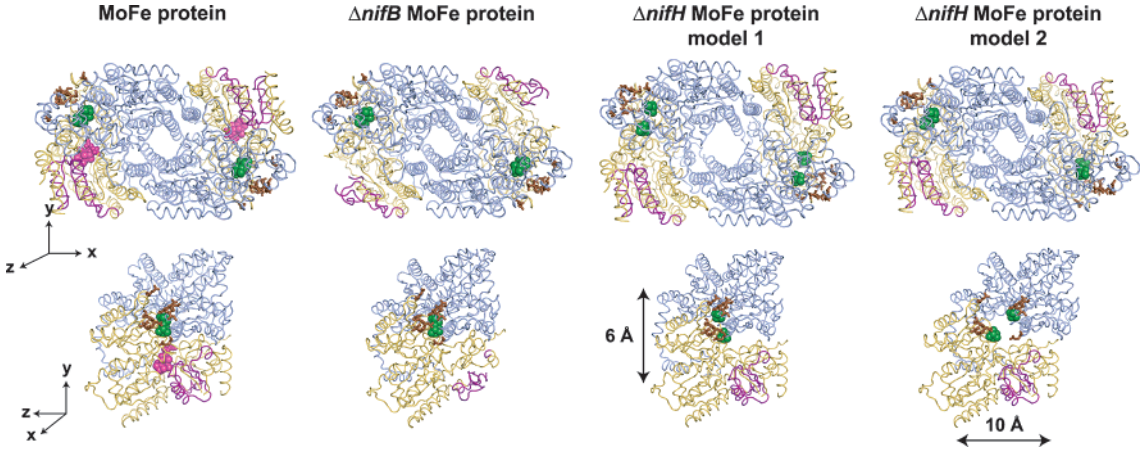

FIGURE 5: Ribbon diagrams of wild-type MoFe protein, Δ*nifB* MoFe protein, and two models consistent with the Δ*nifH* MoFe protein SAXS data. The top row shows a complete $\alpha_2\beta_2$ heterotetramer of each. The bottom row shows a single $\alpha\beta$ heterodimer viewed end-on. The α subunits are colored gold, the β subunits light blue, the residues that rearrange to accommodate insertion of FeMoco into the Δ*nifB* MoFe protein magenta (*17*), and some of the residues that mediate the protein−protein interactions with the Fe protein in a putative nitrogenase turnover complex brown (*36*−*38*). The FeMoco and homocitrate atoms are shown as pink spheres. The P-cluster atoms are shown as green spheres. Wild-type MoFe protein coordinates are from PDB entry 3MIN (*29*). Δ*nifB* MoFe protein coordinates are from PDB entry 1L5H (*17*). Δ*nifH* MoFe protein model 1 was constructed from the wild-type MoFe protein structure by deletion of the FeMoco clusters followed by a symmetric 6 Å translation of the α and β subunits about the *y*-axis. Model 1 is considered to be the best representation of the Δ*nifH* MoFe protein because it has fragmented, solvent-exposed P-clusters and provides a good fit to the SAXS data with a minimum perturbation of the overall MoFe protein structure. Δ*nifH* MoFe protein model 2 was constructed from the wild-type MoFe protein structure by deletion of FeMoco followed by a 10 Å translation of the β subunits along the *z*-axis.

fragmentation.[5] The theoretical scattering profiles from these models were then compared to the Δ*nifH* MoFe protein data. Models formed by rotations of domains within the α and β subunits that did not necessarily impact the P-cluster structure were also analyzed; however, in all cases, the degree of rotation necessary to achieve good matches to the experimental scattering data consistent with the chelation assay results (vida infra) led to structures having significant steric clashes between the residues in different domains.

The Δ*nifH* MoFe protein structure is not anticipated to be extremely different from the wild type because the Δ*nifH* MoFe protein is active in mediating ATP hydrolysis by the Fe protein (*18*), although slight changes would not be precluded, as the Fe protein is active in complexes with nitrogenase proteins that are not identical homologues of the MoFe protein (*13*, *34*, *35*). There are several interaction regions on the surface of the MoFe protein that are involved with Fe protein complex formation leading to ATP hydrolysis, some of which are located at the α subunit−β subunit interface (*36*−*38*). Changes that affect the P-cluster will also affect this Fe protein interaction region; thus, the best models

[5] The wild-type MoFe protein coordinates were used because it is known that Cysα275 is buried in Δ*nifH* MoFe protein as it is in the wild-type protein, but not in Δ*nifB* MoFe protein (*32*).

will be those that provide a good match to the experimental data with a minimal perturbation in the MoFe protein structure. The best theoretical matches to the Δ*nifH* MoFe protein scattering data were calculated from models in which the α and *β* subunits of the MoFe protein were translated along the molecular *y*- or *z*-axes (Figure 4C, sets 3 and 4). These types of movements change the size of the protein without significantly altering its globular shape (see Figure 5, models 1 and 2), consistent with the lack of a large change in the shape of the *p*(*r*) function of this protein relative to that of the wild-type protein. Of the two best models, the *y*-axis-translated structure is considered to be the more reasonable because it represents a smaller overall change in the protein structure (Figure 5, model 1). Only rigid-body translations and rotations of the subunits and domains of the MoFe protein were performed during the search for the best Δ*nifH* MoFe protein structural representation. It is likely that there would be subtler rearrangements in the protein tertiary structure in addition to these large-scale movements. The best model for Δ*nifH* MoFe protein is, therefore, not an exact solution but rather provides a general picture of the large-scale differences between the Δ*nifH* and wild-type or Δ*nifB* MoFe proteins.

The Δ*nifH*^{PI} MoFe protein exhibits a scattering profile very similar to that of the Δ*nifH* MoFe protein at both low and intermediate *h* values (Figures 1B and 3) and is, therefore, expected to have an overall shape similar to that of the Δ*nifH* MoFe protein. Because this protein is similar in shape to the Δ*nifH* MoFe protein, but considered to exist in multiple conformations, theoretical comparisons were not attempted with this data.

Fe Chelation Assay. Previous studies have shown that the Δ*nifH* MoFe protein is more sensitive to heat and gel filtration treatments than the wild-type and Δ*nifB* MoFe proteins (*39*, *40*), which is consistent with it being a less stable tetramer. These results suggest that the α and *β* subunit contacts could be perturbed in the Δ*nifH* MoFe protein concomitant with P-cluster fragmentation. Support for this conclusion and the SAXS-derived model is provided by the results of an Fe chelation assay, which measures the solvent accessibility of the P-cluster Fe atoms in the different FeMoco-deficient MoFe proteins.

When the FeMoco-deficient Δ*nifB* MoFe protein is reacted with the Fe chelator bathophenanthroline disulfonate, almost no Fe is removed from the protein (Figure 6). This lack of chelation is due to the location of the P-cluster in the MoFe protein (it is buried ~10 Å below the protein surface) and not its cluster structure, as the P-cluster Fe atoms are accessible to chelation when the MoFe protein is denatured (*41*, *42*). In contrast, when the FeMoco-deficient Δ*nifH* or Δ*nifH*^{PI} MoFe proteins are reacted with the same chelator, the Fe atoms are rapidly complexed (Figure 6). These results indicate that the Fe atoms of the P-cluster are no longer buried but are instead accessible to solvent in the native state of the Δ*nifH* and Δ*nifH*^{PI} MoFe proteins.

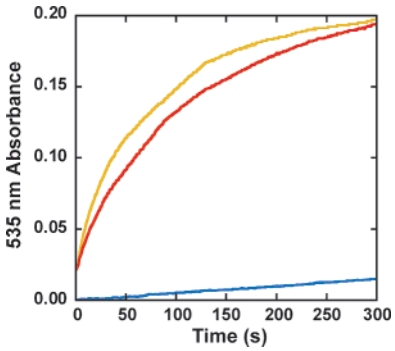

FIGURE 6: Chelation of Fe from the FeMoco-deficient Δ*nifB* (blue), Δ*nifH* (gold), and Δ*nifH*^{PI} (red) MoFe proteins with bathophenanthroline disulfonate. The amount of chelation is measured by the absorbance of the Fe−bathophenanthroline complex at 535 nm. Curves were fitted to single-exponential equations over a period of 20 s, resulting in the following rate constants: 0.0001 s^{-1} for Δ*nifB* MoFe protein, 0.0037 s^{-1} for Δ*nifH* MoFe protein, and 0.0029 s^{-1} for Δ*nifH*^{PI} MoFe protein.

DISCUSSION

SAXS has proven to be a valuable tool for studying the conformations of MoFe proteins in solution. It is sensitive not only to small changes in protein shape but also to the presence or absence of FeMoco. The SAXS results detailed herein have confirmed that there is a connection between the structure of the P-cluster and the conformation of the MoFe protein. The MoFe proteins that contain P-cluster variants, Δ*nifH* MoFe protein and Δ*nifH*^{PI} MoFe protein, are similar in shape but larger than the P-cluster-containing wild-type and Δ*nifB* MoFe proteins. This increase in size is correlated to an increase in the solvent accessibility of the P-cluster Fe atoms and can be modeled well by a 6 Å opening at the α subunit−*β* subunit interface (Figure 5, model 1).

The P-cluster sites may need to be solvent accessible in an immature form of the MoFe protein to enable the initial loading of the α and *β* subunits with the [Fe_4S_4]-like clusters that ultimately become the P-cluster. Once present, the [Fe_4S_4]-like clusters can then be rearranged into the P-cluster during the final assembly of the MoFe protein tetramer. P-Cluster formation and MoFe protein maturation are clearly correlated as mutations in many of the residues that ligate the P-cluster in *K. pneumoniae* MoFe protein result in MoFe proteins with alternate subunit compositions (*43*). Furthermore, proper assembly of the P-cluster can be affected by mutations that disrupt the α subunit−*β* subunit interface without directly impacting the P-cluster site. This was shown by the observation of P-cluster variants in an *A. vinelandii* MoFe protein with a mutation in the FeMoco binding domain at Trpα444 (*44*). In this case, the mutation of Trp to Gly could affect both the H-bonding and *π*-stacking interactions that provide stability to the α subunit−*β* subunit interface, thereby disrupting tetramer assembly and, as a result, P-cluster formation.

The combination of SAXS and chelation studies reported herein with previous spectroscopic studies (*15*, *18*, *19*, *45*) presents a picture of an intermediate in MoFe protein biosynthesis that contains two [Fe_4S_4]-like P-cluster variant clusters separated by an opening at the α subunit−*β* subunit interface of the protein. These results signify that P-cluster formation is associated with MoFe protein tetramer assembly, which suggests an intriguing mechanism for metallocluster biosynthesis that is unavailable to the synthetic inorganic chemist and that relies on using the protein to correctly orient two fragments for condensation into a higher-order cluster. Before MoFe protein maturation can proceed from the Δ*nifH* MoFe protein state, the protein must be rearranged into its more stable wild-type state and the fragment [Fe_4S_4]-like

clusters must be joined to form a subunit-bridging cluster. This process clearly involves the Fe protein, as the immature extended form of the MoFe protein is found in the absence of the gene that encodes the Fe protein, but it also clearly requires additional factors, as the Fe protein alone is not capable of altering the MoFe protein or P-cluster variant structure (*19*). Determining what those additional factors are and how they work together to influence the MoFe protein conformation and assessing the correlation between the rearrangements that close the α subunit−β subunit interface to form the P-cluster and open the α-subunit for FeMoco insertion are the subjects of ongoing investigations.

ACKNOWLEDGMENT

SAXS experimental support was provided by Dr. M. Niebuhr (SSRL). Dr. C. A. Smith (SSRL) aided with protein structure visualization, manipulation, and analysis. Protein concentration determination was carried out with the aid of Dr. K. D. Corbett and Prof. J. M. Berger at the University of California (Berkeley, CA).

REFERENCES

1. Hu, Y., Corbett, M. C., Fay, A. W., Webber, J. A., Hedman, B., Hodgson, K. O., and Ribbe, M. W. (2006) FeMoco Maturation on NifEN, *Proc. Natl. Acad. Sci. U.S.A. 103*, 17119−17124.
2. Ludden, P. W., Shah, V. K., Roberts, G. P., Rüttimann-Johnson, C., Rangaraj, P., Foulger, T., Allen, R. M., Homer, M., Roll, J., Zhang, X., and Chatterjee, R. (1998) Biosynthesis of the Iron-Molybdenum and Iron-Vanadium Cofactors, in *Biological Nitrogen Fixation for the 21st Century* (Elmerich, C., Kondorosi, A., and Newton, W. E., Eds.) pp 33−37, Kluwer Academic Publishers, Dordrecht, The Netherlands.
3. Frazzon, J., and Dean, D. R. (2002) Biosynthesis of the Nitrogenase Iron-Molybdenum-Cofactor from *Azotobacter vinelandii*, in *Metal Ions in Biological Systems* (Sigel, A., and Sigel, H., Eds.) pp 163−186, Marcel Dekker, New York.
4. Rubio, L. M., and Ludden, P. W. (2002) The Gene Products of the *nif* Regulon, in *Nitrogen Fixation at the Millennium* (Leigh, G. J., Ed.) pp 101−136, Elsevier Science, New York.
5. Dos Santos, P. C., Dean, D. R., Hu, Y., and Ribbe, M. W. (2004) Formation and Insertion of the Nitrogenase Iron-Molybdenum Cofactor, *Chem. Rev. 104*, 1159−1173.
6. Rubio, L. M., and Ludden, P. W. (2005) Maturation of Nitrogenase: A Biochemical Puzzle, *J. Bacteriol. 187*, 405−414.
7. Howard, J. B., and Rees, D. C. (1996) Structural Basis of Biological Nitrogen Fixation, *Chem. Rev. 96*, 2965−2982.
8. Burgess, B. K., and Lowe, D. J. (1996) Mechanism of Molybdenum Nitrogenase, *Chem. Rev. 96*, 2983−3011.
9. Smith, B. E. (1999) Structure, Function, and Biosynthesis of the Metallosulfur Clusters in Nitrogenases, *Adv. Inorg. Chem. 47*, 159−218.
10. Igarashi, R. Y., and Seefeldt, L. C. (2003) Nitrogen Fixation: The Mechanism of the Mo-Dependent Nitrogenase, *Crit. Rev. Biochem. Mol. Biol. 38*, 351−384.
11. Rees, D. C., Tezcan, F. A., Haynes, C. A., Walton, M. Y., Andrade, S., Einsle, O., and Howard, J. B. (2005) Structural Basis of Biological Nitrogen Fixation, *Philos. Trans. R. Soc. London, Ser. A 363*, 971−984.
12. Peters, J. W., and Szilagyi, R. K. (2006) Exploring New Frontiers of Nitrogenase Structure and Mechanism, *Curr. Opin. Chem. Biol. 10*, 1−8.
13. Hu, Y., Corbett, M. C., Fay, A. W., Webber, J. A., Hedman, B., Hodgson, K. O., and Ribbe, M. W. (2006) Nitrogenase Fe Protein: A Mo/Homocitrate Insertase, *Proc. Natl. Acad. Sci. U.S.A. 103*, 17125−17130.
14. Corbett, M. C., Hu, Y., Fay, A. W., Ribbe, M. W., Hedman, B., and Hodgson, K. O. (2006) Structural Insights into a Protein-Bound Iron-Molybdenum Cofactor Precursor, *Proc. Natl. Acad. Sci. U.S.A. 103*, 1238−1243.
15. Corbett, M. C., Hu, Y., Naderi, F., Ribbe, M. W., Hedman, B., and Hodgson, K. O. (2004) Comparison of Iron-Molybdenum Cofactor Deficient Nitrogenase MoFe Proteins by X-Ray Absorption Spectroscopy: Implications for P-Cluster Biosynthesis, *J. Biol. Chem. 279*, 28276−28282.
16. Christiansen, J., Goodwin, P. J., Lanzilotta, W. N., Seefeldt, L. C., and Dean, D. R. (1998) Catalytic and Biophysical Properties of a Nitrogenase Apo-MoFe Protein Produced by a *nifB*-Deletion Mutant of *Azotobacter vinelandii*, *Biochemistry 37*, 12611−12623.
17. Schmid, B., Ribbe, M. W., Einsle, O., Yoshida, M., Thomas, L. M., Dean, D. R., Rees, D. C., and Burgess, B. K. (2002) Structure of a Cofactor-Deficient Nitrogenase MoFe Protein, *Science 296*, 352−356.
18. Ribbe, M. W., Hu, Y., Guo, M., Schmid, B., and Burgess, B. K. (2002) The FeMoco-Deficient MoFe Protein Produced by a *nifH* Deletion Strain of *Azotobacter vinelandii* Shows Unusual P-Cluster Features, *J. Biol. Chem. 277*, 23469−23476.
19. Hu, Y., Corbett, M. C., Fay, A. W., Webber, J. A., Hedman, B., Hodgson, K. O., and Ribbe, M. W. (2005) Nitrogenase Reactivity with P-Cluster Variants, *Proc. Natl. Acad. Sci. U.S.A. 102*, 13825−13830.
20. Grossman, J. G., Hasnain, S. S., Yousafzai, F. K., Smith, B. E., Eady, R. R., Schindelin, H., Kisker, C., Howard, J. B., Tsuruta, H., Muller, J., and Rees, D. C. (1999) Comparing Crystallographic and Solution Structures of Nitrogenase Complexes, *Acta Crystallogr. D55*, 727−728.
21. Grossman, J. G., Hasnain, S. S., Yousafzai, F. K., and Eady, R. R. (2001) Evidence for the Selective Population of the FeMo Cofactor Sites in MoFe Protein and its Molecular Recognition by the Fe protein in Transition State Complexes, *J. Biol. Chem. 276*, 6582−6590.
22. Burgess, B. K., Jacobs, D. B., and Stiefel, E. I. (1980) Large-Scale Purification of High Activity *Azotobacter vinelandii* Nitrogenase, *Biochim. Biophys. Acta 614*, 196−209.
23. Tsuruta, H., Brennan, S., Rek, Z. U., Irving, T. C., Tompkins, W. H., and Hodgson, K. O. (1998) A Wide-Bandpass Multilayer Monochromator for Bio SAXS, *J. Appl. Crystallogr. 31*, 672−682.
24. Smolsky, I. L., Liu, P., Niebuhr, M., Ito, K., Weiss, T. M., and Tsuruta, H. (2007) Biological Small-Angle X-Ray Scattering Facility at the Stanford Synchrotron Radiation Laboratory, *J. Appl. Crystallogr. 40*, 453−458.
25. Konarev, P. V., Volkov, V. V., Sokolova, A. V., Koch, M. H. J., and Svergun, D. I. (2003) *PRIMUS*: A Windows PC-Based System for Small-Angle Scattering Data Analysis, *J. Appl. Crystallogr. 36*, 1277−1282.
26. Svergun, D. I. (1992) Determination of the Regularization Parameter in Indirect-Transform Methods Using Perceptual Criteria, *J. Appl. Crystallogr. 25*, 495−503.
27. Koch, M. H. J., Vachette, P., and Svergun, D. I. (2003) Small-Angle Scattering: A View on the Properties, Structures and Structural Changes of Biological Macromolecules in Solution, *Q. Rev. Biophys. 36*, 147−227.
28. Svergun, D. I., Barberato, C., and Koch, M. H. J. (1995) *CRYSOL*: A Program to Evaluate X-Ray Solution Scattering of Biological Macromolecules from Atomic Coordinates, *J. Appl. Crystallogr. 28*, 768−773.
29. Peters, J. W., Stowell, M. H. B., Soltis, S. M., Finnegan, M. G., Johnson, M. K., and Rees, D. C. (1997) Redox-Dependent Structural Changes in the Nitrogenase P-Cluster, *Biochemistry 36*, 1181−1187.
30. DeLano, W. L. (2002) *The PyMOL Molecular Graphics System*, DeLano Scientific, San Carlos, CA.
31. Kim, J., and Rees, D. C. (1992) Crystallographic Structure and Functional Implications of the Nitrogenase Molybdenum-Iron Protein from *Azotobacter vinelandii*, *Nature 360*, 553−560.
32. Angove, H. C., Yoo, S. J., Münck, E., and Burgess, B. K. (1998) An All-Ferrous State of the Fe Protein of Nitrogenase, *J. Biol. Chem. 273*, 26330−26337.
33. Magnuson, J. K., Paustian, T. D., Shah, V. K., Dean, D. R., Roberts, G. P., Rees, D. C., and Howard, J. B. (1997) Nitrogenase Iron-Molybdenum Cofactor Binding Site: Protein Conformational Changes Associated with Cofactor Binding, *Tetrahedron 53*, 11971−11984.
34. Eady, R. R. (1996) Structure-Function Relationships of Alternative Nitrogenases, *Chem. Rev. 96*, 3013−3030.
35. Emerich, D. W., and Burris, R. H. (1978) Complementary Functioning of the Component Proteins of Nitrogenase from Several Bacteria, *J. Bacteriol. 134*, 936−943.
36. Schindelin, H., Kisker, C., Schlessman, J. L., Howard, J. B., and Rees, D. C. (1997) Structure of an ADP·AlF_4^--Stabilized Nitro-

genase Complex and its Implications for Signal Transduction, *Nature 387*, 370−376.
37. Chiu, H.-J., Peters, J. W., Lanzilotta, W. N., Ryle, M. J., Seefeldt, L. C., Howard, J. B., and Rees, D. C. (2001) MgATP-Bound and Nucleotide-Free Structures of a Nitrogenase Protein Complex between the Leu 127Δ-Fe-Protein and the MoFe-Protein, *Biochemistry 40*, 641−650.
38. Tezcan, F. A., Kaiser, J. T., Mustafi, D., Walton, M. Y., Howard, J. B., and Rees, D. C. (2005) Nitrogenase Complexes: Multiple Docking Sites for a Nucleotide Switch Protein, *Science 309*, 1377−1380.
39. Hu, Y., Fay, A. W., Dos Santos, P. C., Naderi, F., and Ribbe, M. W. (2004) Characterization of *Azotobacter vinelandii nifZ*-Deletion Strains: Indication of Stepwise MoFe Protein Assembly, *J. Biol. Chem. 279*, 54963−54971.
40. Tal, S., Chun, T. W., Gavini, N., and Burgess, B. K. (1991) The Δ*nifB* (or Δ*nifE*) FeMo Cofactor-Deficient MoFe Protein is Different from the Δ*nifH* Protein, *J. Biol. Chem. 266*, 10654−10657.
41. Zimmermann, R., Münck, E., Brill, W. J., Shah, V. K., Henzl, M. T., Rawlings, J., and Orme-Johnson, W. H. (1978) Nitrogenase X: Mössbauer and EPR Studies on Reversibly Oxidized MoFe Protein from *Azotobacter vinelandii* OP. Nature of the Iron Centers, *Biochim. Biophys. Acta 537*, 185−207.
42. Kurtz, D. M., Jr., Jack, R. F., McMillan, R. S., Burgess, B. K., Mortenson, L. E., and Holm, R. H. (1979) Identification of Iron-Sulfur Centers in the Iron-Molybdenum Proteins of Nitrogenase, *Proc. Natl. Acad. Sci. U.S.A. 76*, 4986−4989.
43. Kent, H. M., Ioannidis, I., Gormal, C., Smith, B. E., and Buck, M. (1989) Site-Directed Mutagenesis of the *Klebsiella pneumoniae* Nitrogenase, *Biochem. J. 264*, 257−264.
44. Hu, Y., Fay, A. W., Schmid, B., Makar, B., and Ribbe, M. W. (2006) Molecular Insights into Nitrogenase FeMoco Insertion: TRP-444 of MoFe Protein α-Subunit Locks FeMoco in its Binding Site, *J. Biol. Chem. 281*, 30534−30541.
45. Broach, R. B., Rupnik, K., Hu, Y., Fay, A. W., Cotton, M., Ribbe, M. W., and Hales, B. J. (2006) Variable-Temperature, Variable-Field Magnetic Circular Dichroism Spectroscopic Study of the Metal Clusters in the Δ*nifB* and Δ*nifH* MoFe Proteins of Nitrogenase from *Azotobacter vinelandii*, *Biochemistry 45*, 15039−15048.
46. Eady, R. R. (2003) Current Status of Structure Function Relationships of Vanadium Nitrogenase, *Coord. Chem. Rev. 237*, 23−30.
47. Ribbe, M., Gadkari, D., and Meyer, O. (1997) N_2 Fixation by *Streptomyces thermoautotrophicus* Involves a Molybdenum-Dinitrogenase and a Manganese-Superoxide Oxidoreductase That Couple N_2 Reduction to the Oxidation of Superoxide Produced from O_2 by a Molybdenum-CO Dehydrogenase, *J. Biol. Chem. 272*, 26627−26633.
48. Einsle, O., Tezcan, F. A., Andrade, S. L. A., Schmid, B., Yoshida, M., Howard, J. B., and Rees, D. C. (2002) Nitrogenase MoFe-Protein at 1.16 Å Resolution: A Central Ligand in the FeMo-Cofactor, *Science 297*, 1696−1700.

BI7005064